Treadmilling FtsZ polymers drive the directional movement of sPG-synthesis enzymes *via* a Brownian ratchet mechanism

Joshua W. McCausland[1], Xinxing Yang[1], Zhixin Lyu[1], Bill Söderström[2], Jie Xiao[1,*], and Jian Liu[3,*]

1. Department of Biophysics and Biophysical Chemistry, Johns Hopkins School of Medicine, USA;

2. Structural Cellular Biology Unit, Okinawa Institute of Science and Technology, Japan; and The ithree institute, University of Technology Sydney, Ultimo, NSW, 2007 Australia;

3. Department of Cell Biology, Johns Hopkins School of Medicine, USA.

(*) Corresponding Authors: xiao@jhmi.edu and jliu187@jhmi.edu

14 ## Abstract

15

16 FtsZ, a highly conserved bacterial tubulin GTPase homolog, is a central component of
17 the cell division machinery in nearly all walled bacteria. FtsZ polymerizes at the future
18 division site and recruits > 30 proteins that assemble into a macromolecular complex
19 termed divisome. Many of these divisome proteins are involved in septal cell wall
20 peptidoglycan (sPG) synthesis. Recent studies found that FtsZ polymers undergo GTP
21 hydrolysis-coupled treadmilling dynamics along the septum circumference of dividing
22 cells, which drives processive movements of sPG synthesis enzymes. The mechanism
23 of FtsZ treadmilling-driven directional transport of sPG enzymes and its precise role in
24 bacterial cell division are unknown. Combining theoretical modeling and experimental
25 testing, we show that FtsZ treadmilling drives the directional movement of sPG-
26 synthesis enzymes *via* a Brownian ratchet mechanism, where the shrinking end of FtsZ
27 polymers introduces an asymmetry to rectify diffusions of single enzyme molecules into
28 persistent end-tracking movement. Furthermore, we show that processivity of this
29 directional movement hinges on the balance between the enzyme's diffusion and FtsZ's
30 treadmilling speed, which provides a mechanism to control the level of available
31 enzymes for active sPG synthesis, explaining the distinct roles of FtsZ treadmilling in
32 modulating cell wall constriction rate observed in different bacterial species.

33

34

During cell wall constriction in most gram negative bacteria, new septal peptidoglycan (sPG) synthesis and old cell wall degradation occur simultaneously[1]. A large number of cell wall enzymes and their regulators involved in this process has been identified. However, it remains unclear how these proteins are orchestrated in time and space to achieve successful cytokinesis and at the same time maintain the structural integrity of the septal cell wall[2,3]. Perturbations of PG remodeling at septum compromise cell division and often lead to cell lysis[4].

Recent studies have indicated that FtsZ, an essential component of the bacterial cell division machinery, may play a central part in regulating the spatiotemporal coordination of sPG synthesis enzymes. FtsZ is a highly conserved bacterial tubulin homologue and GTPase[5-7]. In *E. coli* during cell division, FtsZ polymerizes at the cytoplasmic face of the inner membrane to form a ring-like structure (Z-ring) at mid-cell[8-10]. The Z-ring then locally recruits an ensemble of more than 30 proteins, many of which are sPG-remodeling enzymes[1,11], to initiate septal cell wall constriction. New studies employing super-resolution and single-molecule imaging *in vitro* and *in vivo* have demonstrated that the FtsZ polymers exhibit GTP hydrolysis-driven treadmilling dynamics, which are the continuous polymerization at one end and depolymerization at the other end, with individual FtsZ monomers remaining stationary in the middle[12,13]. Most interestingly, it was found that FtsZ's treadmilling dynamics drives processive movements of the essential sPG transpeptidase (TPase, FtsI in *E. coli* and PBP2B in *B. subtilis*)[12,13] and glycosyltransferase FtsW[14]. Consequently, it was proposed that the

58 FtsZ's treadmilling dynamics spatially and temporally distribute sPG synthesis enzymes
59 along the septum plane to ensure smooth septum morphogenesis[13]. However, it is
60 unknown how FtsZ's treadmilling dynamics with stationary monomers in the cytoplasm
61 are transduced into the periplasm to drive the persistent and directional movement of
62 cell wall synthesis enzymes. The role of FtsZ's treadmilling dynamics in modulating sPG
63 synthesis activity also remains elusive, as it was shown that the cell wall constriction
64 rate is dependent on FtsZ's treadmilling speed in *B. subtilis*[12] but not in *E. coli*[13], *S.*
65 *aureus* or *S. pneumoniae*[15,16].
66
67 In this work, we combined agent-based theoretical modeling with single-molecule
68 imaging-based experimental testing to address the mechanism involved in FtsZ
69 treadmilling-dependent processive movement of sPG enzymes and the associated role
70 in bacterial cell division. We found that a Brownian ratchet mechanism underlies the
71 persistent and directional movement of single sPG synthesis enzyme molecules (using
72 FtsI as the model) driven by FtsZ's treadmilling dynamics. Most importantly, the
73 processivity of the Brownian ratchet is modulated by the balance between FtsI's random
74 diffusion and FtsZ's treadmilling speed. This finding indicates that different bacterial
75 species could harness the same FtsZ treadmilling machinery – but modulate diffusions
76 of sPG synthesis enzymes – to achieve distinct processivities of sPG enzymes and
77 control their availability for sPG synthesis. As such, FtsZ's treadmilling dynamics impact
78 the rate of cell wall constriction differentially in different species. Given the lack of linear
79 stepping motors in the prokaryotic world, our work suggests a general framework on
80 how polymer dynamics coupled with Brownian-ratcheting could underlie directional

transport of cargos and be shaped by evolution to meet the needs of different cellular milieus.

Results

Model description

Our model is based on the concept of a Brownian Ratchet, where FtsZ's treadmilling events introduce an asymmetry to bias the random diffusion of FtsI molecules in the periplasm, upon which FtsI persistently follows the shrinking end of a treadmilling FtsZ filament (Fig. 1). The quantitative details of the model are rooted in the physical and chemical properties of key components of the system, which can be well characterized by experiments.

As shown in Fig. 1, the model describes the movement of a FtsI molecule at the septum as a quasi-1D problem. The model assumes that FtsI, the essential TPase with a single transmembrane domain and a cytoplasmic tail, can freely diffuse along the inner membrane at the septum or interact indirectly with the treadmilling FtsZ filament underneath the inner membrane (Fig. 1A). The dynamics of a single FtsI molecule at septum is thus determined by three parameters, the constant of FtsI's free diffusion (D), the treadmilling speed (V_Z) of FtsZ filaments, and the attraction force determined by the binding potential (U) between FtsI and FtsZ (Fig. 1B and C). The diffusion constant of FtsI in *E. coli* and PBP2B in *B. subtilis* were measured to be in the range of ~ 10^{-3}–10^{-1} $\mu m^2/s$ using single-molecule tracking (SMT)[17,18]; the average treadmilling speed of FtsZ

was at ~ 20 – 40 nm/s *in vivo* but can be a few-folder faster *in vitro*, therefore we set a large range of 10 – 100 nm/s[19,20]. FtsI interacts with FtsZ at septum indirectly through a relay of protein-protein interactions that include FtsN, FtsA, and/or FtsEX[1,21]. For simplicity we omit the details of the protein-protein interaction relay but refer to it as the interaction between FtsI and FtsZ. The indirect interaction between a FtsZ monomer and a nearby FtsI molecule constitute an attractive force for each other and can be described as a short-ranged harmonic binding potential (Fig. 1C). We assumed the potential range at ± 2.5 nm, commensurate with the size of a FtsZ monomer (~ 5 nm)[22-25], and the potential's magnitude at ~10 k_BT, corresponding to a K_d in the μM range, which is typical for protein-protein interactions in the bacterial divisome system[26-30].

To numerically compute the model, we describe the dynamics of FtsI by a Langevin-type equation (equation (1)) where the viscous drag force on the molecule is in balance with a driving force *f* and a force from thermal noise ξ:

$$\lambda \frac{dx(t)}{dt} = f\big(x(t)\big) + \xi(t) \qquad \text{Equation (1)}$$

Here, $x(t)$ represents the location of a FtsI molecule at time t along the 1D septum. λ is the effective viscous drag coefficient for FtsI's movement with $\lambda = k_BT/D$, where D is the diffusion constant of the free FtsI on the inner membrane when it is not interacting with FtsZ. $f(x(t))$ is the attractive force exerted upon the FtsI molecule by the FtsZ binding potential, $U(x, t)$ (Fig. 1C). Specifically, $f(x(t)) = -\partial U(x, t)/\partial x$ at time t. The last term $\xi(t)$

reflects the random diffusive motion of the FtsI on the inner membrane with $\langle \xi(t) \cdot \xi(t') \rangle = 2D \cdot \Delta t \cdot \delta(t - t')$, where Δt is the unitary time step in simulation.

Next, we simulate the shrinking of a FtsZ filament according to equation (2), which describes how the position of the shrinking end of a treadmilling FtsZ filament at time t, $x_Z(t)$, is related to the shrinking rate, V_Z,

$$\frac{dx_Z(t)}{dt} = V_Z \qquad \text{Equation (2)}$$

Each time when a FtsZ subunit falls off from the shrinking end of the filament, the associated binding potential vanishes with it.

To discern principal interactions, the model only considers one FtsI molecule and one FtsZ filament in a self-contained septal section. Hereby, we do not consider complicated cases, in which the movement of one FtsI molecule may be interfered by different FtsZ filaments undergoing treadmilling in the same or opposite directions. Further, we do not consider FtsI molecules that are bound to the middle of FtsZ filaments, as these FtsI molecules will either diffuse away, or eventually start end-tracking FtsZ filaments when the shrinking end of the treadmilling FtsZ filament approaches. These complicated scenarios can be decomposed into the elementary process elucidated by the model.

Assuming that the FtsZ filament treadmills from left to right with a steady-state length of ~ 200 nm, the model implements a hard-wall boundary condition on the FtsI molecule at the left edge of the system, while keeping the right edge as an open boundary so that the right-ward FtsZ treadmilling is not limited. We also note that the model results

148 presented below reflect the nominal case, whose essence remains robust against the
149 variations of the model parameters within the physical range constrained by existing
150 experimental data.
151
152 **A Brownian-ratchet mechanism can couple FtsI's directional movement to FtsZ's**
153 **treadmilling dynamics**
154
155 As we described above, Brownian-ratcheting hinges on the diffusion of FtsI, its
156 interaction with FtsZ, and FtsZ's treadmilling speed. To examine how the movement of
157 FtsI depends on FtsI's diffusion and the binding potential between FtsI and FtsZ, we
158 kept FtsZ's treadmilling speed constant at an experimentally measured 25 nm/s and
159 carried out a phase diagram study using stochastic simulations. We chose a parameter
160 range of 0.0001 to 0.1 $\mu m^2/s$ for FtsI's diffusion based on commonly measured diffusion
161 constants for bacterial inner membrane proteins[17,18]. The upper limit of the binding
162 potential was set ~ 20 k_BT, which corresponded to a dissociation constant K_d in the nM-
163 range.
164
165 We considered an initial condition in which both the shrinking end of a FtsZ filament and
166 a FtsI molecule were at the left boundary of the septal section. To be commensurate
167 with our experimental analysis, we counted a FtsI trajectory as being moving
168 directionally if it tracked the shrinking end of a treadmilling FtsZ filament persistently and
169 unidirectionally for ≥ 4 seconds. Because of the stochastic nature of Brownian
170 ratcheting, if 50% or more of simulated FtsI trajectories displayed such a persistent

171 directional movement, we characterized the state of FtsI under this parameter set
172 condition as persistent end-tracking in the phase diagram.
173
174 As shown in the phase diagram in Fig. 2A, the model showed that when the binding
175 potential between FtsZ and FtsI was weak (< 5 k_BT, ~ mM Kd), FtsI largely displayed
176 random diffusion without directional movements along the septum. When the attraction
177 potential was sufficiently strong (> 5 k_BT), strong binding quenched free diffusions and
178 confined FtsI to the end of a FtsZ filament. As the FtsZ subunit at the shrinking end of
179 the filament fell off, the next one in the row attracted and coupled FtsI, which pulled FtsI
180 to the right by ~ 5 nm. With the subsequent FtsZ subunits falling off one after the other
181 from the shrinking end, the FtsI molecule ratcheted forward and stably tracked the end
182 of the treadmilling FtsZ filament. These consecutive movements resulted in a persistent
183 and directional trajectory of FtsI with 5-nm sub-steps (Fig. 2B). Consequently, the speed
184 of FtsI directional movement was tightly coupled to FtsZ's treadmilling speed (Fig. 2C),
185 recapitulating the experimentally measured nearly linear correlation between FtsI's
186 directional moving speed with FtsZ's treadmilling speeds in both wildtype and FtsZ
187 GTPase mutants[13].
188
189 The phase diagram also showed that at a constant binding potential between FtsZ and
190 FtsI, persistent end-tracking of FtsI required an appropriate range of diffusion constant
191 (Fig. 2A). If FtsI diffused too rapidly, it could not be confined by the binding potential of
192 the shrinking end of the FtsZ filament. Conversely, when FtsI diffused too slowly, it
193 would not be able to keep up with the speed of departing FtsZ subunits at the shrinking

194 end. Once falling behind, the FtsI molecule would lose the contact with the left most
195 FtsZ subunits permanently.
196
197 Taken together, the phase diagram analysis showed that the Brownian-ratchet
198 mechanism was able to couple FtsI's directional movement to FtsZ's treadmilling within
199 the parameter range that is well consistent with experimentally measured data, *i.e*,
200 0.001 to 0.1 $\mu m^2/s$ for FtsI's diffusion coefficient, > 5 k_BT for the binding potential
201 between FtsI and FtsZ, and at the *in vivo* FtsZ treadmilling speed of ~ 25 nm/s. Further,
202 the same model could explain the nondirectional movement of the other divisome
203 protein FtsN in a recent *in vitro* study[19]. In that study, the cytoplasmic tail of FtsN was
204 reported to follow the tracks of treadmilling FtsZ filaments on a supported lipid bilayer at
205 the ensemble level. At the single molecule level, however, the FtsN tail only binds and
206 unbinds FtsZ filaments transiently but does not exhibit directional movement[26]. Such a
207 scenario could be explained by to our Brownian ratchet model in that the diffusion of
208 free FtsN cytoplasmic tail anchored on the membrane was too large (0.3 – 0.6 $\mu m^2/s$)[19]
209 to be confined by the binding potential of FtsZ.
210
211 **FtsZ's treadmilling speed modulates processivity of FtsI's end-tracking**
212
213 Next, we investigated how FtsZ's treadmilling speed impacts the processivity of FtsI's
214 directional movement. Addressing this question will help us understand the role of
215 FtsZ's treadmilling dynamics in the spatial organization and/or regulation of sPG
216 synthesis activity. We focused on three features that collectively defined the processivity

of FtsI's end-tracking: (1) the propensity, (2) the run distance, and (3) the duration of persistent end-tracking trajectories.

We first examined how the propensity of FtsI's persistent end-tracking was modulated by FtsZ treadmilling speed. Here we define the propensity as the percentage of FtsZ trajectories that showed > 4s directional movement in all simulated trajectories under each parameter set. Keeping the diffusion constant of FtsI at 0.01 $\mu m^2/s$ and the binding potential at 10 k_BT, stochastic simulations of the Brownian ratchet model predicted that when the FtsZ treadmilling speed was < 50 nm/s, nearly all simulated FtsI trajectories displayed persistent end-tracking (Fig. 3A). However, as the FtsZ treadmilling speed increased beyond 50 nm/s, the percentage of persistent end-tracking trajectories of FtsI dropped off sharply to 60% at 75 nm/s, and further to 20% at 100 nm/s (Fig. 3A). That is, when the FtsZ treadmilling was too fast, FtsI could not couple FtsZ shrinking end in most cases and became largely diffusive.

To further this point, we calculated the phase diagram of FtsI's persistent end-tracking propensity as a function of both FtsI's diffusion constant and FtsZ treadmilling speed (Fig. 3B), while keeping the binding potential fixed at 10 k_BT. Again, we used a 50% FtsI persistent end-tracking trajectories as the criterium for the phase boundary. As shown in Fig. 3B, for a fixed diffusion constant of FtsI, there was an upper limit of FtsZ's treadmilling speed that FtsI could persistently couple. Conversely, for a fixed FtsZ treadmilling speed, persistent end-tracking of FtsI required an appropriate range of diffusion constants. Importantly, a very large diffusion constant of FtsI (> 0.1 $\mu m^2/s$) did

not support persistent end-tracking irrespective of FtsZ's treadmilling speed. These results were consistent with the phase diagram in Fig. 2A and the recent *in vitro* study of FtsN's cytoplasmic tail[26].

Next, we investigated how FtsZ's treadmilling speed modulates the run distance and duration of FtsI's persistent end-tracking. The Brownian ratchet model predicted that both the run length and duration of FtsI's persistent end-tracking should display broad distributions due to the stochastic nature of FtsI's diffusion and the interaction between FtsI and FtsZ. Moreover, the model predicts that when FtsZ's treadmilling speed increase, the duration of FtsI's persistent end-tracking will decrease (Fig. 3C), whereas the run distance will display a biphasic dependence that peaks around an intermediate FtsZ treadmilling speed (~ 50 nm/s at the current parameter setting, Fig. 3D). Importantly, such distinctive dependences of duration and run distance on FtsZ treadmilling speed is a natural consequence of the Brownian ratchet mechanism (Supplementary Info). Qualitatively speaking, when a FtsZ subunit falls off from the shrinking end of the FtsZ filament, the associated FtsI molecule will either diffuse away or catch up with the next FtsZ subunit in the row to continue end-tracking, the latter depending on how fast FtsZ treadmills. When FtsZ treadmills too fast (for example > 50 nm/s), it will be difficult for FtsI to catch up (Fig. 3A), resulting in early termination of end-tracking, and hence both the persistence run distance and duration will be short. When FtsZ treadmills relatively slowly (< 50 nm/s), the probability of FtsI catching up with the shrinking end of the FtsZ filament is high (Fig. 3A). Therefore, the persistence run distance will be proportional to the FtsZ treadmilling speed as predicted in Fig. 3D.

Within the same time window, however, when FtsZ treadmills slowly, an end-tracking FtsI molecule would face fewer number of dissociation events, and hence there is a lower chance for FtsI to diffuse away to terminate the trajectory, leading to a longer duration of persistence run compared to the regime when FtsZ treadmills relatively fast (but still < 50 nm/s). One can imagine in the extreme case where FtsZ does not treadmill at all (V_Z = 0), the duration of persistence runs would then be mainly dictated by the intrinsic dissociation rate of FtsI from FtsZ, and the persistence run distance would be the shortest (i.e., the size of a single FtsZ subunit). An analytical proof of these relationships was provided in Supplementary Information and Extended Data Fig. 1.

Single-molecule tracking of FtsI confirms model predictions

To experimentally examine the model's predictions as described above, we performed single-molecule tracking (SMT) of a functional sandwich fusion protein FtsI-Halo^{SW} labeled with JF646 in live *E. coli* cells[31,32]. To avoid disrupting the cytoplasmic interactions of FtsI's N-terminal tail with other divisome proteins, we inserted the Halo tag between the last residue (18) of the N-terminal cytoplasmic tail and the first residue of the inner membrane helix (19) of FtsI (Fig. 4Ai). We integrated the *ftsI-halo*^{SW} fusion gene into the chromosome replacing the endogenous *ftsI* gene and showed that it was expressed as a full-length fusion protein and supported normal cell division indistinguishable from wild-type (WT) cells (Extended Data Fig. 2).

To obtain precise measurements of the persistence run distance and duration of single FtsI-Halo^{SW} molecules, we trapped individual *E. coli* cells vertically in agarose microholes made using cell-shaped nanopillar molds as previously described[33,34] so that the entire circumference of the septum could be visualized at the same focal plane (Fig. 4Aii). To determine whether a FtsI-Halo^{SW} molecule was at a septum, we labeled the FtsZ-ring using an ectopically expressed GFP-ZapA fusion protein, which we and others have previously shown as a faithful marker of the Z-ring localization and dynamics[35]. The GFP-ZapA image also allowed us to unwrap the circular trajectories of FtsI-Halo molecules along the septum to linear displacements along the circumference of the septum, from which we could measure the persistent run speed, distance, and duration (Fig. 4Aiii-v).

As shown in Fig. 4B, the directional moving speed of FtsI-Halo exhibited a wide distribution as we previously showed for FtsZ's treadmilling. Consistent with our prediction (Fig. 3A), the occurrence of FtsI's directional movement decreases significantly as the speed is > 40 nm/s. Most excitingly, the persistence run distance and duration exhibited precisely the same trends as what was predicted by the model: while the run duration decreased monotonically (Fig. 4C), the persistence run length increased and then decreased when FtsI's speed increased (Fig. 4D). Note here that we inferred FtsZ's treadmilling speed from FtsI's directional moving speed due to the difficulty in the two-color co-tracking experiment, although we have demonstrated previously that these two were linearly coupled[13]. Also note that one potential caveat in these experiments was that a very fast FtsZ treadmilling speed (*i.e.*, > 80 nm/s) is rare

in wildtype *E. coli* cells as we showed previously and here by the FtsI speed distribution. Therefore, given the relatively small dataset for high speed FtsZ treadmilling, our data may not be definitive to distinguish whether the FtsI couldn't effectively end-track fast FtsZ treadmilling or there were simply not many fast FtsZ treadmilling events in the first place. Nevertheless, the agreement of our experimental measurements with theoretical predictions supported the validity of the Brownian rachet model.

Brownian ratchet mechanism explains the differential dependence of sPG synthesis activity on FtsZ treadmilling speed in different bacterial species

In *E. coli*, the total amount of septal PG synthesis and the septum constriction rate are insensitive to perturbations in FtsZ's treadmilling speed from ~ 8 nm/s to ~ 30 nm/s in a series of FtsZ GTPase mutants[13]. This insensitivity suggests that end-tracking, directional moving FtsI molecules were unlikely active in sPG synthesis. Thus, the functional role of FtsZ's treadmilling in *E. coli* is proposed to spatially control the location of sPG synthesis by acting as a shuttle to transport sPG synthase molecules along the septum without affecting their enzymatic activity[13]. In *B. subtilis*, however, it was shown that the constriction time positively correlated with FtsZ's treadmilling speed, suggesting that the faster FtsZ treadmills, the more sPG synthesis activity there is[12]. Many factors have been proposed to explain why there is such a difference, such as cell wall synthesis precursor levels, species-specific protein-protein interactions, septal cell wall compositions or cell wall constriction stages, but none has been confirmed. As we show below, the interplay between the diffusion of synthase molecules and FtsZ's treadmilling

speed in the Brownian ratchet model determines the fraction of active sPG synthases, which naturally gives rise to the differential dependence of sPG synthesis activity on FtsZ's treadmilling speed.

To illustrate the interplay between the diffusion of synthase molecules and FtsZ's treadmilling, we first determined the fraction of time a FtsI molecule spent in persistent end-tracking (termed "fraction of end-tracking") at different FtsZ treadmilling speeds. The fraction of end-tracking is defined as the time a FtsI molecule continuously end-tracks the shrinking end of a FtsZ filaments divided by the total time simulated, which is typically 60 s. As shown in Fig. 5A, when FtsI diffused relatively fast (~ 0.05 $\mu m^2/s$, dashed line with triangle), the fraction of time FtsI molecules spent in end-tracking was largely insensitive to FtsZ's treadmilling speed so that it only decreased from 99% to 91% when the corresponding FtsZ treadmilling speed increased 3-fold from ~ 8 nm/s to 25 nm/s. In contrast, when FtsI diffused relatively slowly, the fraction of time FtsI molecules spent in end-tracking not only reduced significantly as compared to that of faster diffusion but was critically dependent by FtsZ treadmilling speed. For example, at a diffusion constant of 0.003 $\mu m^2/s$, the fraction of end-tracking FtsI molecules decreased from 73% to 24% when FtsZ treadmilling speed increased from ~ 8 nm/s to 25 nm/s (continuous line with circle). The physical reason behind this drastic difference between fast and slow FtsI diffusion lies at the core of Brownian ratchet mechanism. A fast diffusion will allow FtsI to catch up with the shrinking end of a FtsZ filament in very short time (Fig. 5B). When FtsI's diffusion becomes slower and slower, it eventually becomes the rate-limiting factor in the Brownian ratchet–more than often the slow FtsI

354 molecules falls behinds the FtsZ shrinking end and takes a long time to catch up with
355 the shrinking end of a departing FtsZ filament, or simply just diffuses away and become
356 lost (Fig. 5C). As such, further increasing the FtsZ treadmilling speed in the latter case
357 will significantly reduce the chance of FtsI keeping up with the FtsZ shrinking end and,
358 hence the percentage of end-tracking.
359
360 Exploiting the above results could allow us to explain the differences between *E. coli*
361 and *B. subtilis*. Consider that the fraction of time a FtsI molecule end-tracks reflects the
362 overall fraction of all FtsI molecules that are associated with treadmilling FtsZ filaments
363 at the septum. As we previously showed in *E. coli* that the FtsZ treadmilling-driven
364 population of FtsI are not active in sPG synthesis, it follows that the active FtsI
365 population would be proportional to the fraction released from treadmilling FtsZ
366 filaments. Therefore, FtsZ's treadmilling speed could modulate the amount of sPG
367 synthases that would be available for synthesis in different bacterial species depending
368 on the diffusion of sPG synthase molecules.
369
370 In *E. coli*, we observed that the sPG synthesis activity was insensitive to FtsZ's
371 treadmilling speed from 8 nm/s to ~ 30 nm/s in a series of FtsZ GTPase mutants[13]. This
372 insensitivity could be explained by the Brownian rachet model if the diffusion of FtsI in *E.*
373 *coli* is fast enough so that there is negligible change in the fraction of end-tracking FtsI
374 molecules when FtsZ's treadmilling speed changes as that predicted in Fig. 5A (dash
375 line with triangle). To examine this possibility, we performed single-molecule tracking of
376 FtsI again using a faster frame rate (20 Hz) in order to capture freely diffusing molecules.

The mean-square-displacement (MSD) analysis showed that the apparent diffusion constant of FtsI in wildtype *E. coli* cells was ~ 0.024 $\mu m^2/s$ (Fig. 5D), well within the predicted range in Fig. 5A and similar to the measured diffusion constant of PBP1b [18]. In contrast, the TPase PBP2B diffused ~ 10-fold slower in *B. subtilis* (~ 0.003 $\mu m^2/s$) than that in *E. coli*[17,18], likely due to more viscous septal environment in *B. subtilis* than that in *E. coli*. The slow diffusion of PBP2B leads to the highly sensitive curve of the fraction of time of PBP2B spent in end-tracking on FtsZ's treadmilling speed as shown in Fig. 5A (continuous line with circle). As FtsZ's treadmilling speed increases, there will be reduced levels of end-tracking PBP2B molecules, leading to increased levels of available PBP2B molecules for active sPG synthesis, and hence faster septal cell wall constriction.

Discussion

We note that other mechanisms (but not necessarily exclusive from the Brownian Ratchet model) could also be at play. For instance, detailed molecular interactions among the septal ring complexes might be regulated distinctly to fulfil the different functional requirements in different systems. After all, the sPG synthesis in *B. subtilis* needs to produce a cell wall of ~ 10 times thicker than *E. coli* (~ 50 nm vs. ~ 5 nm)[36,37]. This may relate to the fact that the septal ring components are typically several-fold more abundant in *B. subtilis* than those in *E. coli*[12]. Nevertheless, our results in *E. coli* points to a mechanistic possibility that the same Brownian-ratchet machinery may be at work in *B. subtilis* but operate in a different regime of the parameter space. This

possibility precipitates further questions: What are the differences in sPG synthesis and cell division between *E. coli* and *B. subtilis*? How does the coupling between sPG synthesis complexes and FtsZ treadmilling adapt to the different systems? There could be many possible evolutionary routes revolving around these issues. For instance, a thicker cell wall and/or a more crowded periplasm – perhaps due to the presence of more abundant PG synthesizing-proteins – may slow down FtsI diffusion. A slower FtsI diffusion will in turn reduce the percentage of end-tracking FtsI which are inactive in sPG synthesis (Fig. 5A). Reciprocally, there will be more fraction of FtsI molecules active in PG-synthesis, meeting the requirement for producing a thicker cell wall. From evolutionary standpoint, is a thicker cell wall the cause or the result of a slower FtsI diffusion? Is it an emergent phenomenon of sPG synthesis being proportional to FtsZ treadmilling speed in *B. subtilis*? After all, FtsZ not only localizes the sPG-synthesizing enzymes to the septum but could also regulate the available level of enzymes for sPG synthesis by controlling the FtsZ treadmilling speed (Figs. 5A-C). This way, the chemical energy of FtsZ GTPase hydrolysis is harnessed “purposely” for bacterial cell division.

We further note that in addition to *E. coli* and *B. subtilis*, other bacteria seem to adopt more diverse strategies of exploiting FtsZ treadmilling in sPG synthase activity and cell division. For instance, in *S. aureus*, it was observed that septum constriction was dependent on FtsZ’s treadmilling initially but becomes independent at a later stage[38]. In *S. pneumoniae*, the directional movement of the synthase complex was found to be completely independent of FtsZ’s treadmilling[15]. It will be in our future work to

423 interrogate whether and how the Brownian-ratchet mechanism plays out under these
424 different contexts. In a broader scope, given the lack of linear stepper motors in
425 prokaryotic world, Brownian-ratcheting appears to be an ancient mechanism for directed
426 cargo transportation in bacteria – another salient example is ParA-mediated DNA
427 partitioning[39-41]. Interestingly, a similar Brownian-ratchet mechanism also underlies
428 directional movements of mitotic chromosomes by end-tracking spindle microtubule in
429 eukaryotes[42]. Can we distill unified fundamental principle(s) by which evolution shapes
430 the same Brownian-ratchet mechanism to meet distinct needs under different contexts?
431 We will relegate these exciting quests in our near-future study.

Acknowledgements

The authors would like to thank members in the Xiao and S. Holden labs for helpful discussions and technical assistance, Dr. G. Hauk for sharing plasmids and the CRISPR-Cas9/λ-red recombineering cloning method, R. McQuillen for help cloning pRM027, Dr. E. Goley for help with growth curve measurements, and Dr. L. Lavis for sharing JF646. This work was supported in part by NIH GM007445 (to J.W.M.), NIH R01 GM086447 (to J.X.), GM125656 (subcontract to J. X.), NSF EAGER Award MCB-1019000 (to J.X.), a Hamilton Smith Innovative Research Award (to J.X .), Johns Hopkins University Startup fund (to J.L.) and Catalyst Awards (to J.L.).

Author Contributions

J.W.M., X.Y and Z.L performed experiments. J.L. carried out theoretical modeling. All authors contributed to concept development, data analysis, and manuscript writing.

Competing interests

The authors declare no competing interests.

Reference

1 Egan, A. J. F. & Vollmer, W. The physiology of bacterial cell division. *Annals of the New York Academy of Sciences* **1277**, 8-28, doi:10.1111/j.1749-6632.2012.06818.x (2013).

2 de Pedro, M. A. & Cava, F. Structural constraints and dynamics of bacterial cell wall architecture. *Frontiers in Microbiology* **6**, doi:10.3389/fmicb.2015.00449 (2015).

3 Typas, A., Banzhaf, M., Gross, C. A. & Vollmer, W. From the regulation of peptidoglycan synthesis to bacterial growth and morphology. *Nature Reviews Microbiology* **10**, 123, doi:10.1038/nrmicro2677 (2011).

4 Schmidt, L. S., Botta, G. & Park, J. T. Effects of furazlocillin, a beta-lactam antibiotic which binds selectively to penicillin-binding protein 3, on Escherichia coli mutants deficient in other penicillin-binding proteins. *Journal of Bacteriology* **145**, 632-637 (1981).

5 de Boer, P., Crossley, R. & Rothfield, L. The essential bacterial cell-division protein FtsZ is a GTPase. *Nature* **359**, 254-256, doi:10.1038/359254a0 (1992).

6 RayChaudhuri, D. & Park, J. T. Escherichia coli cell-division gene ftsZ encodes a novel GTP-binding protein. *Nature* **359**, 251-254, doi:10.1038/359251a0 (1992).

7 Löwe, J. & Amos, L. A. Crystal structure of the bacterial cell-division protein FtsZ. *Nature* **391**, 203-206, doi:10.1038/34472 (1998).

8 Bi, E. & Lutkenhaus, J. FtsZ ring structure associated with division in Escherichia coli. *Nature* **354**, 161-164, doi:10.1038/354161a0 (1991).

9 Hale, C. A. & de Boer, P. A. J. Direct Binding of FtsZ to ZipA, an Essential Component of the Septal Ring Structure That Mediates Cell Division in E. coli. *Cell* **88**, 175-185, doi:https://doi.org/10.1016/S0092-8674(00)81838-3 (1997).

10 Pichoff, S. & Lutkenhaus, J. Unique and overlapping roles for ZipA and FtsA in septal ring assembly in Escherichia coli. *The EMBO Journal* **21**, 685-693, doi:10.1093/emboj/21.4.685 (2002).

11 Haeusser, D. P. & Margolin, W. Splitsville: structural and functional insights into the dynamic bacterial Z ring. *Nature Reviews Microbiology* **14**, 305, doi:10.1038/nrmicro.2016.26 (2016).

12 Bisson-Filho, A. W. *et al.* Treadmilling by FtsZ filaments drives peptidoglycan synthesis and bacterial cell division. *Science* **355**, 739-743, doi:10.1126/science.aak9973 (2017).

13 Yang, X. *et al.* GTPase activity–coupled treadmilling of the bacterial tubulin FtsZ organizes septal cell wall synthesis. *Science* **355**, 744-747, doi:10.1126/science.aak9995 (2017).

14 Yang, X. *et al.* FtsW exhibits distinct processive movements driven by either septal cell wall synthesis or FtsZ treadmilling in E. coli. *bioRxiv*, 850073, doi:10.1101/850073 (2019).

15 Perez, A. J. *et al.* Movement dynamics of divisome proteins and PBP2x:FtsW in cells of Streptococcus pneumoniae. *Proceedings of the National Academy of Sciences* **116**, 3211-3220, doi:10.1073/pnas.1816018116 (2019).

16 Monteiro, J. M. *et al.* Peptidoglycan synthesis drives an FtsZ-treadmilling-independent step of cytokinesis. *Nature* **554**, 528-532, doi:10.1038/nature25506 (2018).

17 Cho, H. *et al.* Bacterial cell wall biogenesis is mediated by SEDS and PBP polymerase families functioning semi-autonomously. *Nature Microbiology* **1**, 16172 (2016).

18 Lee, T. K., Meng, K., Shi, H. & Huang, K. C. Single-molecule imaging reveals modulation of cell wall synthesis dynamics in live bacterial cells. *Nature Communications* **7**, 13170 (2016).

19 Loose, M. & Mitchison, T. J. The bacterial cell division proteins FtsA and FtsZ self-organize into dynamic cytoskeletal patterns. *Nature Cell Biology* **16**, 38, doi:10.1038/ncb2885 (2013).

20 Ramirez-Diaz, D. A. *et al.* Treadmilling analysis reveals new insights into dynamic FtsZ ring architecture. *PLOS Biology* **16**, e2004845, doi:10.1371/journal.pbio.2004845 (2018).

21 Du, S. & Lutkenhaus, J. Assembly and activation of the Escherichia coli divisome. *Molecular Microbiology* **105**, 177-187, doi:10.1111/mmi.13696 (2017).

22 Li, Z., Trimble, M. J., Brun, Y. V. & Jensen, G. J. The structure of FtsZ filaments in vivo suggests a force‐generating role in cell division. *The EMBO Journal* **26**, 4694-4708, doi:10.1038/sj.emboj.7601895 (2007).

23 Löwe, J. & Amos, L. A. Tubulin‐like protofilaments in Ca^{2+}‐induced FtsZ sheets. *The EMBO Journal* **18**, 2364-2371, doi:10.1093/emboj/18.9.2364 (1999).

24 Erickson, H. P., Taylor, D. W., Taylor, K. A. & Bramhill, D. Bacterial cell division protein FtsZ assembles into protofilament sheets and minirings, structural homologs of tubulin polymers. *Proceedings of the National Academy of Sciences* **93**, 519-523, doi:10.1073/pnas.93.1.519 (1996).

25 Oliva, M. A., Cordell, S. C. & Löwe, J. Structural insights into FtsZ protofilament formation. *Nature Structural & Molecular Biology* **11**, 1243-1250, doi:10.1038/nsmb855 (2004).

26 Baranova, N. *et al.* FtsZ assembles the bacterial cell division machinery by a diffusion-and-capture mechanism. *bioRxiv*, 485656, doi:10.1101/485656 (2018).

27 Zou, Y., Li, Y. & Dillon, J.-A. R. The distinctive cell division interactome of Neisseria gonorrhoeae. *BMC Microbiology* **17**, 232, doi:10.1186/s12866-017-1140-1 (2017).

28 Gerding, M. A. *et al.* Self-Enhanced Accumulation of FtsN at Division Sites and Roles for Other Proteins with a SPOR Domain (DamX, DedD, and RlpA) in Escherichia coli Cell Constriction. *Journal of Bacteriology* **191**, 7383-7401, doi:10.1128/jb.00811-09 (2009).

29 Glas, M. *et al.* The Soluble Periplasmic Domains of Escherichia coli Cell Division Proteins FtsQ/FtsB/FtsL Form a Trimeric Complex with Submicromolar Affinity. *Journal of Biological Chemistry* **290**, 21498-21509, doi:10.1074/jbc.M115.654756 (2015).

30 Müller, P. *et al.* The Essential Cell Division Protein FtsN Interacts with the Murein (Peptidoglycan) Synthase PBP1B in Escherichia coli. *Journal of Biological Chemistry* **282**, 36394-36402, doi:10.1074/jbc.M706390200 (2007).

31 Grimm, J. B. *et al.* A general method to improve fluorophores for live-cell and single-molecule microscopy. *Nature Methods* **12**, 244-250, doi:10.1038/nmeth.3256 (2015).

32 Los, G. V. *et al.* HaloTag: A Novel Protein Labeling Technology for Cell Imaging and Protein Analysis. *ACS Chemical Biology* **3**, 373-382, doi:10.1021/cb800025k (2008).

33 Söderström, B., Chan, H., Shilling, P. J., Skoglund, U. & Daley, D. O. Spatial separation of FtsZ and FtsN during cell division. *Molecular Microbiology* **107**, 387-401, doi:10.1111/mmi.13888 (2018).

34 Söderström, B., Badrutdinov, A., Chan, H. & Skoglund, U. Cell shape-independent FtsZ dynamics in synthetically remodeled bacterial cells. *Nature Communications* **9**, 4323, doi:10.1038/s41467-018-06887-7 (2018).

35 Buss, J. *et al.* A Multi-layered Protein Network Stabilizes the Escherichia coli FtsZ-ring and Modulates Constriction Dynamics. *PLOS Genetics* **11**, e1005128, doi:10.1371/journal.pgen.1005128 (2015).

36 Labischinski, H., Goodell, E. W., Goodell, A. & Hochberg, M. L. Direct proof of a "more-than-single-layered" peptidoglycan architecture of Escherichia coli W7: a neutron small-angle scattering study. *Journal of Bacteriology* **173**, 751-756, doi:10.1128/jb.173.2.751-756.1991 (1991).

37 Hayhurst, E. J., Kailas, L., Hobbs, J. K. & Foster, S. J. Cell wall peptidoglycan architecture in Bacillus subtilis. *Proceedings of the National Academy of Sciences* **105**, 14603-14608, doi:10.1073/pnas.0804138105 (2008).

38 Monteiro, J. M. *et al.* Peptidoglycan synthesis drives an FtsZ-treadmilling-independent step of cytokinesis. *Nature* **554**, 528, doi:10.1038/nature25506 (2018).

39 Hu, L., Vecchiarelli, A. G., Mizuuchi, K., Neuman, K. C. & Liu, J. Directed and persistent movement arises from mechanochemistry of the ParA/ParB system. *Proceedings of the National Academy of Sciences* **112**, E7055-E7064, doi:10.1073/pnas.1505147112 (2015).

40 Hu, L., Vecchiarelli, A. G., Mizuuchi, K., Neuman, K. C. & Liu, J. Brownian Ratchet Mechanism for Faithful Segregation of Low-Copy-Number Plasmids. *Biophysical Journal* **112**, 1489-1502, doi:https://doi.org/10.1016/j.bpj.2017.02.039 (2017).

41 Hu, L., Vecchiarelli, A. G., Mizuuchi, K., Neuman, K. C. & Liu, J. Brownian ratchet mechanisms of ParA-mediated partitioning. *Plasmid* **92**, 12-16, doi:https://doi.org/10.1016/j.plasmid.2017.05.002 (2017).

42 Liu, J. & Onuchic, J. N. A driving and coupling “Pac-Man” mechanism for chromosome poleward translocation in anaphase A. *Proceedings of the National Academy of Sciences* **103**, 18432-18437, doi:10.1073/pnas.0608962103 (2006).

584 **Figure 1**

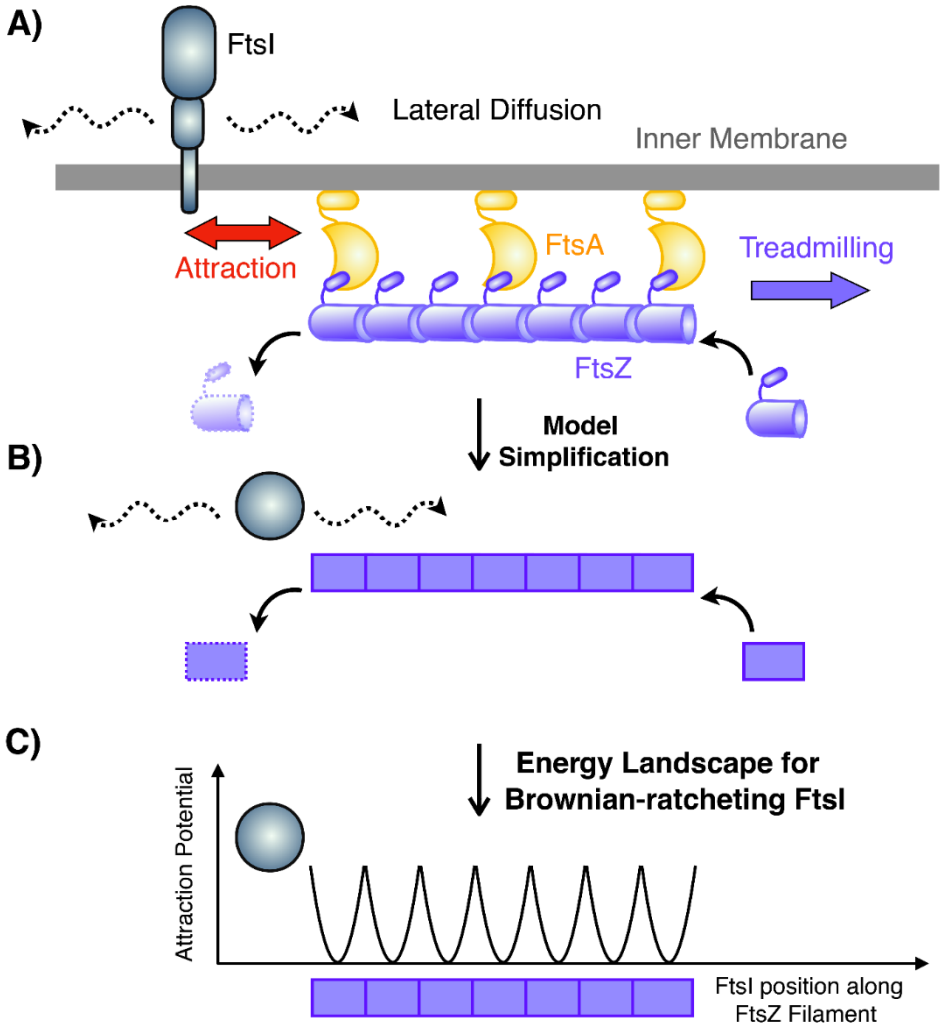

585

586 **Figure 1.** Model description. A) Schematic representation of sPG synthase complex's
587 interaction with FtsZ treadmilling. B) Model simplification of FtsZ – FtsI interaction at the
588 septum. The FtsZ filament (purple) undergoes treadmilling by dissociating FtsZ subunit
589 from the left end and associating new ones from the right end. While the FtsI complex
590 (grey) intrinsically diffuses around, it has binding affinity to FtsZ subunits. C) Schematics
591 of FtsZ – FtsI binding potentials. Here, the binding potential is assumed to be harmonic
592 and short-ranged (~ 5 nm), which is about the size of the individual FtsZ subunit.

593

Figure 2

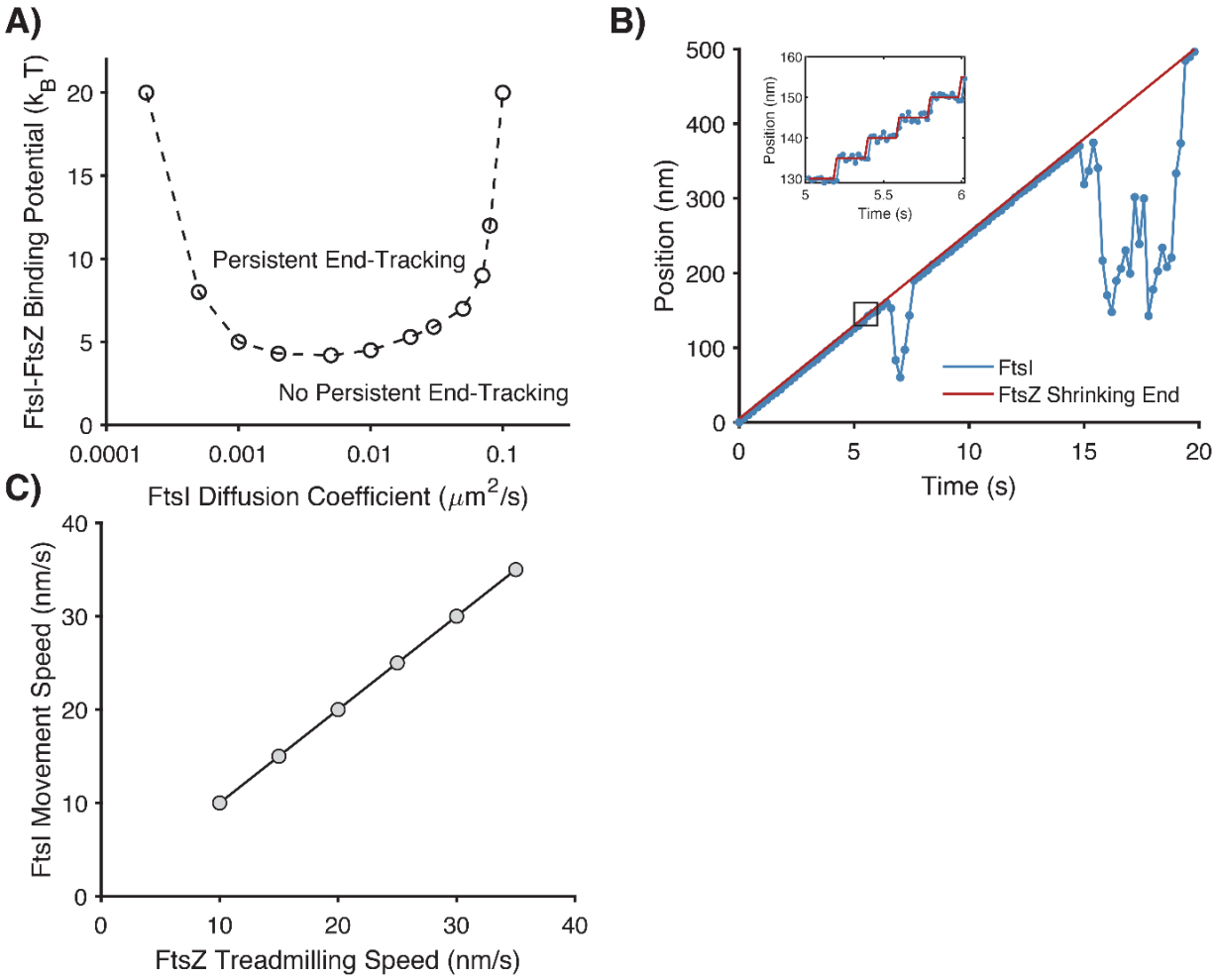

Figure 2. FtsZ treadmilling-mediated Brownian ratchet mechanism drives FtsI directional movement. A) Calculated phase diagram – Dependence of FtsI motilities on FtsI diffusion constant and FtsI-FtsZ binding potential. B) A representative simulated trajectory of FtsI persistent end-tracking with FtsZ treadmilling. Here, the model is simulated with following parameters: FtsZ treadmilling speed is 25 nm/sec, the FtsI diffusion constant is 0.01 μm^2/s, and the FtsZ–FtsI binding potential is 10 k_BT. Inset: A zoom-in view of the trajectory. Here, the simulation time step is 10^{-5} s, the model results are plotted every 10^{-1} s, and those in the zoom-in inset are plotted every 2×10^{-2} s. C) FtsI directional speed tightly couples with FtsZ treadmilling speed. The model calculated

605 the FtsI speed only from the part of its trajectory that the FtsI undergoes persistent end-
606 tracking. Therefore, the FtsI speed varies very little as long as FtsZ treadmilling speed is
607 fixed.
608

609 **Figure 3**

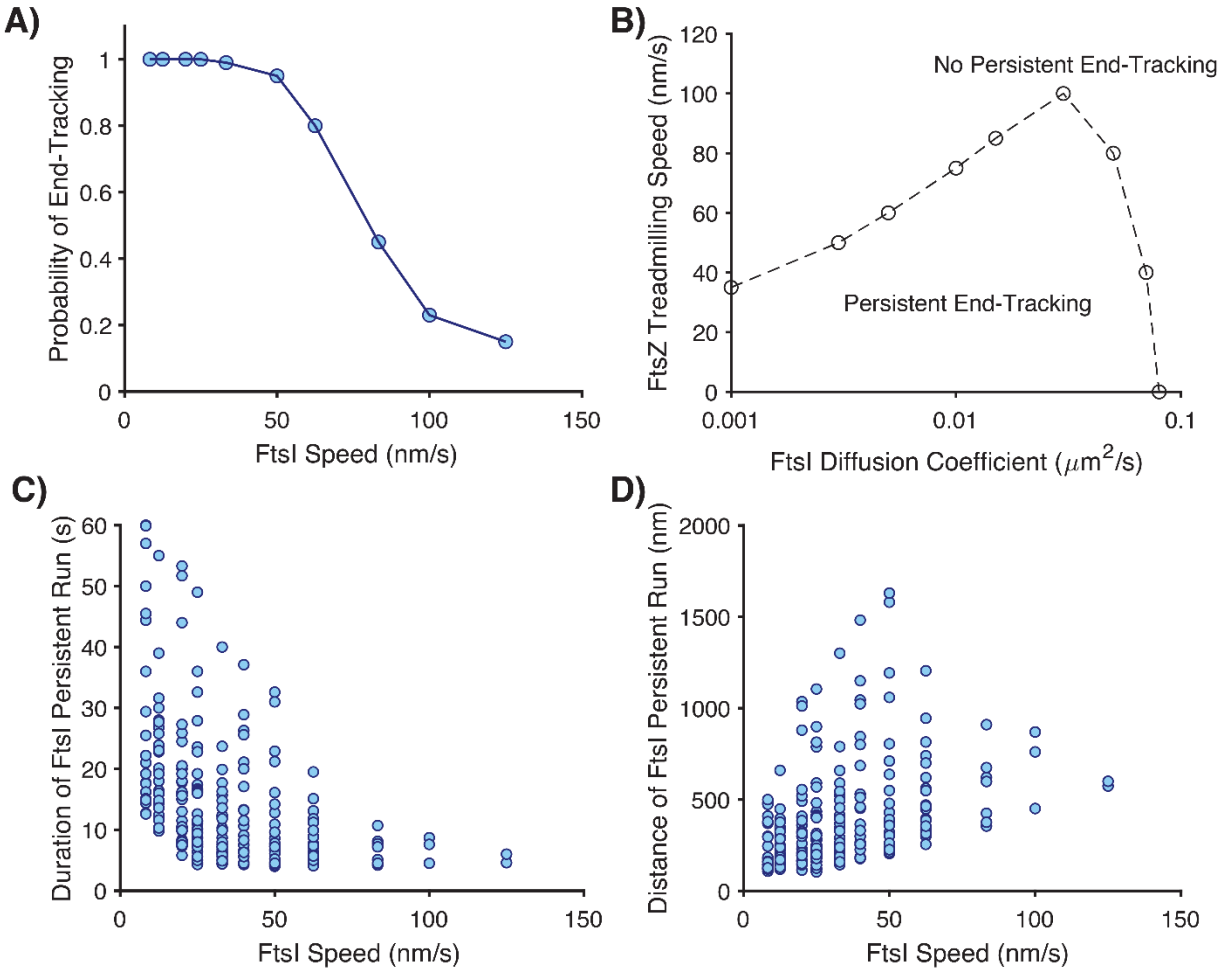

610

611 **Figure 3.** Model predictions on the processivity of FtsI directional movement modulated
612 by FtsZ treadmilling speed. A) Predicted propensity of FtsI persistent end-tracking as a
613 function of FtsZ treadmilling speed. B) Calculated phase diagram of FtsI persistent end-
614 tracking characterized by FtsI diffusion constant and FtsZ treadmilling speed. C)
615 Predicted FtsZ treadmilling speed-dependence of run distance of FtsI persistent end-
616 tracking. D) Predicted FtsZ treadmilling speed-dependence of duration of FtsI/W
617 persistent end-tracking. For the model calculations in (A-D), the FtsZ–FtsI binding
618 potential is set to be 10 k_BT.

619

620 **Figure 4**

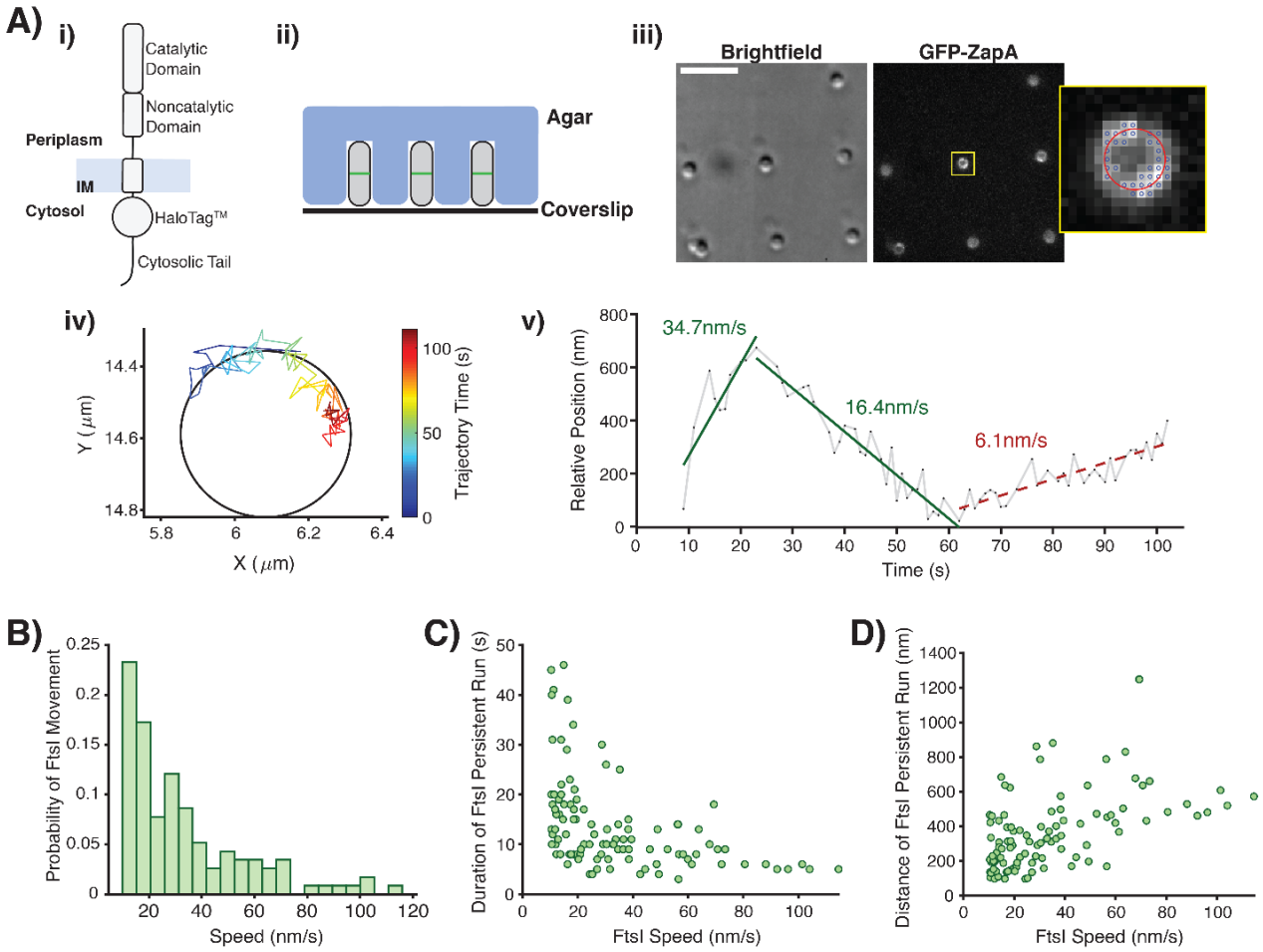

621

622 **Figure 4.** Experimental characterization of FtsI directional movements. A) Single
623 molecule tracking experimental setup. i, Schematics of the fully functional sandwich
624 fusion of FtsI. ii, schematics of individual *E. coli* cells loaded in microholes; iii, brightfield
625 and fluorescence images of microholes loaded with E. coli cells labeled with GFP-ZapA
626 and FtsI-Halo^{SW} fusion proteins. Inset shows the zoomed image of one cell in the yellow
627 box with a circle fit to its intensity profile. iv, GFP-ZapA circle-fit super-imposed with the
628 trajectory of a single FtsI molecule; v the unwrapped trajectory from iv with fitted lines at
629 each segments to extract directional speeds Fitting the directional mobile events allow
630 us to identify movement states in our trajectories. Note that only movement events >10

631 nm/s were used for analysis in this work (fitted lines) because we recently showed that
632 the slow-moving population (average speed ~ 8 nm/s) is independent of FtsZ's
633 treadmilling[14]. B) Histogram of FtsI directional movement speeds. C) Dependence of the
634 duration of FtsI's persistent run on its speed. D) Dependence of the distance of FtsI's
635 persistent run on its speed.
636

637 **Figure 5**

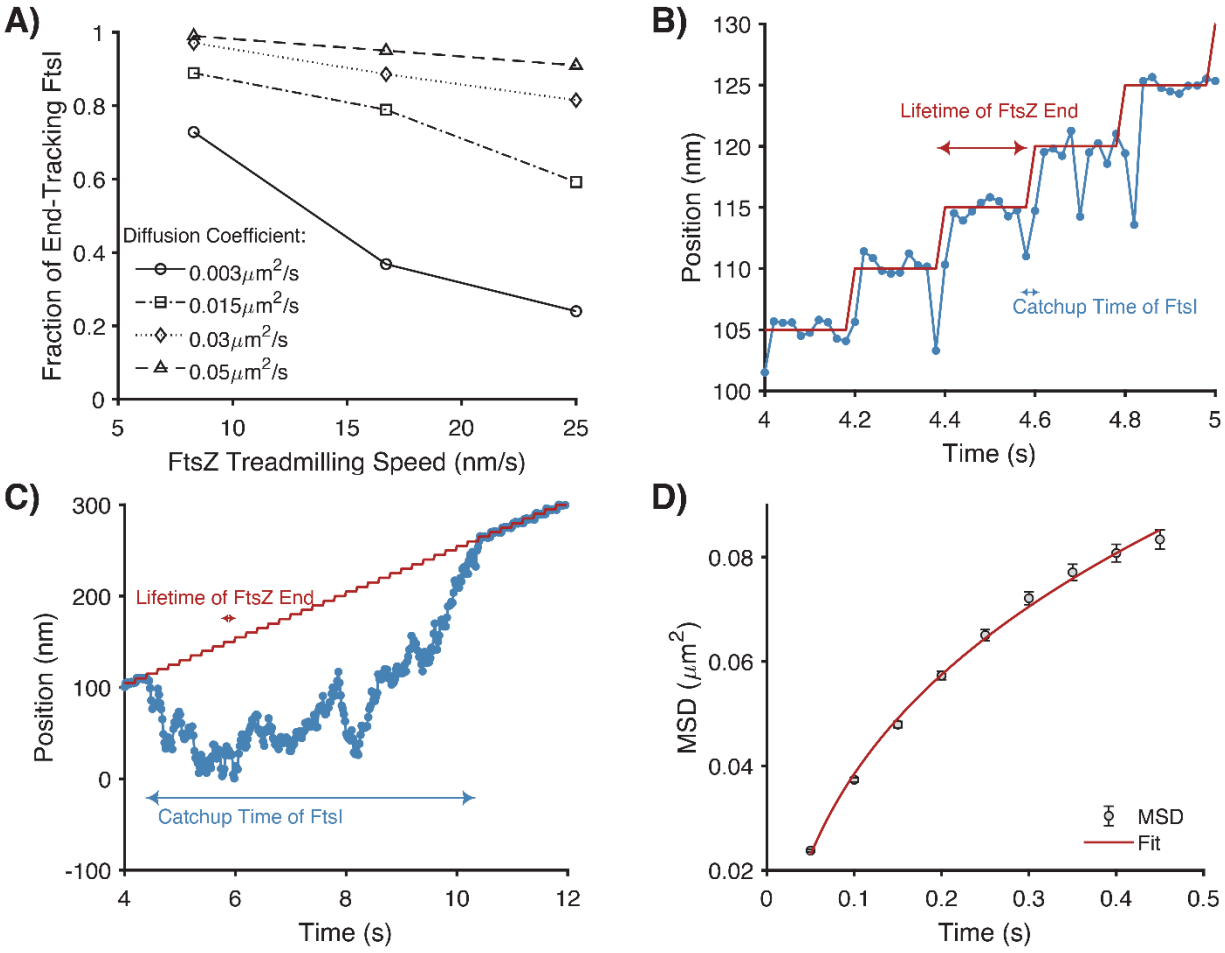

638

639 **Figure 5.** Dependence of FtsI's processivity on its diffusion. A) Predicted dependence
640 of the fraction of end-tracking of FtsI on FtsZ treadmilling speed. The fraction of end-
641 tracking is defined as the percentage of time that FtsI persistently end-tracks FtsZ
642 treadmilling within 60 seconds. B) A representative trajectory of FtsI's persistent end-
643 tracking when FtsI diffusion is fast. C) A representative trajectory of FtsI's persistent
644 end-tracking when the FtsI diffusion is slow. For (B and C), a fast diffusion allows FtsI to
645 catch up with the shrinking end of FtsZ almost immediately, whereas it takes a long time
646 for FtsI to catch up (if it eventually catches up) when it diffuses slowly. Here, the
647 simulation time step is 10^{-5} s, the model results are plotted are plotted every 2×10^{-2} s. D)

Measured MSD of FtsI as a function of time in wildtype *E. coli* cells. From these data, A diffusion constant of FtsI at 0.036 ± 0.001 $\mu m^2/s$ was determined by fitting the MSD curve with function $MSD = 4Dt^{\alpha}$ with $\alpha = 0.42 \pm 0.05$ (standard error from fitting).